Specific capacitance behavior of Co-Co_3O_4 nanocomposite thin films synthesized via different electrodeposition modes

Rania Afia Nuamah, Saleema Noormohammed, Dilip Kumar Sarkar*

Department of Applied Science, University of Quebec at Chicoutimi, Aluminum Research Center-REGAL, Chicoutimi, Quebec, G7H 2B1, Canada

*Corresponding author: dsarkar@uqac.ca

Keywords: Electrodeposition, Pulse reverse potential (PRP), Cyclic voltammetry (CV), Potentiostatic (PS), Co-Co_3O_4 nanocomposite thin film, Supercapacitor electrode, Specific capacitance

Abstract

High capacitance Co-Co_3O_4 nanocomposite thin films have been synthesized on nickel foam (NF) using cyclic voltammetry (CV), combination of cyclic voltammetry and potentiostatic (CV PS –1.4V and CV PS +1V) and combination of cyclic voltammetry and pulse reverse potential (CV PRP) modes of electrodeposition. X-ray diffraction (XRD) studies reveal the presence of Co and Co_3O_4 phases for the four electrodeposition modes. The scanning electron microscope (SEM) revealed an interesting morphology correlating the electrochemical and capacitance behavior while the energy-dispersive X-ray spectroscopy (EDX) spectra confirmed the varying quantities of Co and O in the Co-Co_3O_4 nanocomposite thin films. The presence of Co-O bonds were also confirmed by the attenuated total reflection – Fourier transform infrared (ATR – FTIR) spectra obtained on these films. The capacitance values of Co-Co_3O_4 composite thin films obtained by CV, CV

PS –1.4V, CV PS +1V and CV PRP, respectively, were found to be 1661, 1400, 1866, 2580 F/g at an applied current load of 1 A/g while the capacitance retentions after 500 cycles under a high current load of 20 A/g for the same were 85.8, 77.8, 87.1, and 90.5 %, respectively. The high capacitance and their retention of the electrodeposited Co-Co_3O_4 nanocomposite thin films shows potentials as high-performance supercapacitor electrode.

1 | INTRODUCTION

Advanced technological devices including portable electronics such as mobile phones, tablets, laptops, smart watches as well as low emission technologies including hybrid vehicles constantly demand for light weight energy storage systems for easy portability and handling with long service life. Supercapacitors demonstrate high potential as efficient energy storage systems owing to their most essential features such as light weight, high energy density, high power density, fast charge-discharge rates, easy and safe operation, and long cycle stability [1-3]. Among an array of supercapacitor electrode materials such as activated carbon, conducting polymers and transition metal oxides (TMOs) [4, 5], TMOs are widely preferred due to their high electronegativity and variable oxidation states of metal ions facilitating redox reactions, charge storage, low cost, environmental friendliness and excellent electrochemical performance [2, 4, 6]. TMOs have higher specific capacitance (100–2000 F/g), higher energy density than carbon materials, and better chemical stability than conductive polymers [7]. Noble TMOs such as RuO_2, exhibit high theoretical capacitance and rapid faraday redox reaction proving as optimal pseudocapacitive electrode material, however, are very expensive and environmentally unfriendly, limiting industrial scale productions. Base TMOs, on the other hand, including. Co_3O_4, MnO_2, Fe_2O_3, SnO_2, and ZnO are easy to fabricate and exhibit high theoretical specific capacitance showing potentials as substitutes for RuO_2 [2, 7, 8]. Among these base TMOs, Co_3O_4 has a very high theoretical specific capacitance of 3560 F/g and is relatively low in cost owing to easy fabrication methods [9-11]. Also, nanostructured Co_3O_4 coatings have been found to be useful in other types of applications such electrocatalysts for hydrogen evolution reaction[12] and photocatalysts for discoloration of organic dye contaminants in wastewater and antibacterial treatment [13].

Despite the high theoretical capacitance of Co_3O_4, this TMO suffers limited practical utility due to low experimental capacitance values of this material compared to the theoretical value [14]. Studies have shown that the morphology, structure and dimensions of Co_3O_4 features are easily tunable by controlling the preparative parameters of the fabrication method employed [7, 15, 16]. This is a very important factor in supercapacitive performance as the specific capacitance of the cobalt oxide strongly depends on morphology, surface area, and size distribution contributing to enhancement in the specific surface area, facilitating the electrolyte ion transport in the material [2]. Co_3O_4 with morphological features in nanoscale dimensions can essentially lead to tunable specific surface area in enhancing the experimental specific capacitance values.

Generally, nanostructured Co_3O_4 materials have been prepared by techniques such spray pyrolysis, precipitation, sol-gel, and hydrothermal synthesis. These techniques require the use of binders and conductive materials which increase the electrode resistance affecting their supercapacitance performance [17, 18]. Recently, electrodeposition has become a useful technique for growing Co-O nanostructures with desired composition and morphology directly onto the substrates without necessitating the use of binders. In electrodeposition, several factors such as electrolyte composition, temperature, type of electrodeposition mode, duration of the electrode deposition process, etc., can be adjusted to obtain the desired morphology and texture such as nanoporous structure, nanocolumnar structure, nanoflower-like structure [19-21]. Studies have also reported variation in surface morphology and respective supercapacitive behavior of Co_3O_4 based electrodes by performing electrodeposition in different modes, namely, cyclic voltammetry (CV), potentiostatic (PS), galvanostatic (GS), pulse (current or potential) [15, 22]. Optimal electrodeposition modes together with the appropriate cobalt salt precursor for the preparation of Co_3O_4 based electrodes offering high capacitance closest to the theoretical value as well as low electric resistance, however, needs further investigation.

In view of optimizing the mode of electrodeposition in achieving highest and stable specific capacitance, we have deposited Co-Co_3O_4 nanocomposite thin films electrodes on nickel foam substrates using CV, CV PS -1.4V, CV PS +1V and CV combined with pulsed reverse potential (CV PRP) modes from an electrolyte composed of $CoCl_2$ and

$Co(CH_3COO)_2$ salts solution. The structural, morphological and compositional analyses present a correlation with the electrochemical behavior namely the CV, EIS and charge-discharge cycles. CV PRP mode that led to the deposition of Co-Co_3O_4 nanocomposite thin film is found to present a very high capacitance of 2580 F/g with stable cycling performance.

2 | MATERIALS AND METHODS

In the electrochemical deposition process, the use of a negative potential reduces the Co^{2+} ions into a metallic Co as a film. Similarly, the use of a positive potential deposits a layer of Co_3O_4. In our experiment, a maximum negative potential of -1.4V was used to deposit metallic Co film and a +1.0V was used to deposit Co_3O_4. Cobalt-cobalt oxide (Co-CoO_x) nanocomposite thin films were electrodeposited on nickel foam (NF) substrates by different modes, namely, (1) Cyclic voltammetry (CV), (2) CV followed by potentiostatic (PS) at +1.0 V (CV PS +1.0 V), (3) CV followed by PS at –1.4 V (CV PS –1.4V) and (4) CV followed by pulse reverse potential (CV PRP) cycled between -1.4V and +1.0V. The thin films deposited via these four modes have been identified as Type 1 (CV), Type 2 (CV PS +1.0V), Type 3 (CV PS -1.4V) and Type 4 (CV PRP). CV mode was conducted in a potential range of –1.4 to +1.0 V vs Ag/AgCl at a scan rate of 20 mVs^{-1} for 2 cycles. For the CVPS +1V mode, CV was initially conducted in a potential range of –1.4 to +1.0 V vs Ag/AgCl at a scan rate of 20 mVs^{-1} for 2 cycles, and was followed by potentiostatic deposition at +1 V for 30 s. A similar condition was used for the CV PS –1.4V mode, however with a negative constant potential of –1.4 V. For the CV PRP mode, CV was initially performed in a potential range of –1.4 to +1.0 V vs Ag/AgCl at a scan rate of 20 mVs^{-1} for 2 cycles, followed by pulse reverse potential (PRP) of 60 cycles of width of 1 s for a total duration of 60 s. The minimum and the maximum of pulse heights were chosen to be –1.4 V and +1 V, respectively. The electrolyte solutions used for the electrodeposition consist of 0.1 M cobalt acetate ($Co(CH_3CO_2)_2 \cdot 4\ H_2O$, 6 ml), 0.1 M cobalt chloride ($CoCl_2$ 24 ml) and 0.2 M sodium perchlorate ($NaClO_4.H_2O$, 30 ml). The pH of the electrolyte was 6.5. Prior to the electrodeposition process, the NF substrate was etched in 3 M HCl for 15 minutes and rinsed ultrasonically with ethanol and deionised water for 15 minutes each.

The deposition process was conducted in a standard three-electrode glass cell with a platinum wire, NF substrate and Ag/AgCl as the counter, working and reference electrodes, respectively. After electrodeposition, the as-prepared Co-CoO_x nanocomposite thin film electrodes were rinsed in deionized water and dried in air on a hot plate at 200^o C for 45 minutes before performing characterization and electrochemical analyses. The experimental details of the four electrodeposition modes have been summarized in Table 1. A separate set of samples were also prepared by depositing the thin films on Ti substrate for the purpose of physical characterization by XRD.

Table 1. Summary of the different modes of electrodeposition]

Identification	Electrodeposition mode*	Potential range
Type 1	CV	–1.4V to +1.0V
Type 2	CV PS 1.0V	CV followed by PS at +1.0 V
Type 3	CV PS –1.4V	CV followed by PS at –1.4 V
Type 4	CV PRP	CV followed by PRP of 60 cycles between -1.4V and +1.0V

*****CV – Cyclic voltammetry, PS – potentiostatic, PRP – pulse reverse potential*

The morphological and elemental analyses of the electrodeposited thin films were studied by a scanning electron microscope (SEM, JEOL JSM-6480 LV), equipped with energy-dispersive X-ray spectroscopy (EDX) for elemental analyses. The X-ray diffraction (XRD) analyses were carried out by Bruker D8 Discover system for crystallographic analysis. An attenuated total reflection – Fourier transform infrared spectroscopy (ATR-FTIR, Agilent Technologies Cary 630) was used to confirm and quantify the deposition of the metal oxide (Co-O). The electrochemical properties, namely, cyclic voltammetry (CV) and galvanostatic charge-discharge (GCD) and electrochemical impedance spectroscopy (EIS) characteristics were evaluated using a three- electrode glass cell and Solartron

SI1287 electrochemical workstation with 1 M KOH aqueous electrolyte. The as-synthesized Co-Co_3O_4 nanocomposite thin films on NF substrate of the various types were directly employed as working electrodes, with platinum wire and Hg/HgO as counter and reference electrodes respectively. The CV and GCD measurements were performed at different scan rates and specific currents in a potential window of 0 to 0.6 V and -0.1 to 0.5 V respectively. Additionally, the EIS measurement was conducted in a frequency range from 10 mHz to 100 kHz.

3 | RESULTS AND DISCUSSION

Figure 1 shows the profiles of electrodeposition modes individually for the preparation of the Co-Co_3O_4 nanocomposite thin films on nickel foam (NF) substrates. Electrodeposition of four types of thin films were realised using individual modes: (1) Type 1 (CV, Figure 1(a)), (2) Type 2 (combination of CV and PS (+1.0V), Figure 1(b)), (3) Type 3 (combination of CV and PS (-1.4V), Figure (1(c)), and (4) Type 4, (combination of CV and PRP (between +1.0V and -1.4V), Figure (1(d)). The Type 1 thin film was deposited on NF by using the CV process alone as shown in Figure (1 (a). During this process, the potential is swept between –1.4 to +1.0V, and hence it can be assumed that metal (Co) and metal oxides (Co-O) are deposited on NF simultaneously. A negative potential was used in order to initiate the deposition of metallic Co on NF to enhance the adhesion of the nanocomposite thin film layer deposited further by PS and PRP processes. The Type 2 thin film was deposited utilising CV process followed by PS (+1.0V) by combining Figure 1(a) and 1(b) processes in order to deposit an additional layer of cobalt oxide after the CV process. Similarly, the Type 3 thin film was deposited by CV process followed by PS (–1.4V) to deposit an additional layer of metal (Co). This was achieved by combining the processes shown in Figure 1(a) and 1(c). The Type 4 thin film, on the other hand, was deposited utilising CV process followed by PRP with the potential cycled between –1.4V and +1.0V in order to deposit multilayers of cobalt and cobalt oxide in a sequence where metal deposition is followed by metal oxide deposition after the CV process. This was achieved by combining Figure 1(a) and 1(d).

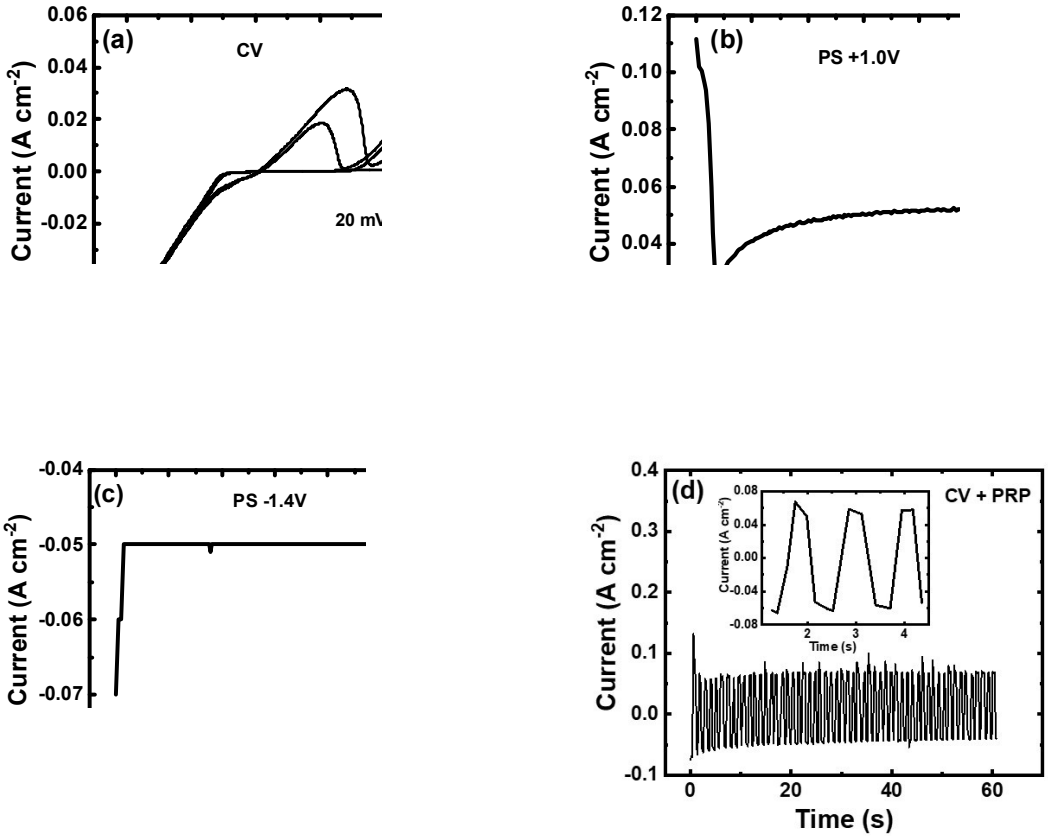

Figure 1 Individual profiles of electrodeposition modes for the preparation of the Co-Co_3O_4 nanocomposite thin films on NF: (a) cyclic voltammetry (CV, 2 scans), (b) potentiostatic at +1.0V (PS +1.0V), (c) potentiostatic at –1.4 V (PS –1.4V), (d) pulse reverse potential (PRP) (inset of (d) shows the current vs. time graph of the first three cycles)

Figure 2(a) shows the XRD patterns of the Co-Co_3O_4 nanocomposite thin films prepared by the four electrodeposition modes on Ti-substrate. The diffraction peaks at 2θ angles of 41.7° and 47.5° are assigned to Co (100) and Co (101) planes of hexagonal crystal structure of cobalt (JCPDS card No-00-005-0727). The peak at 44.6° is assigned to Co_3O_4(400) plane of cubic crystal structure of cobalt oxide (Co_3O_4) (JCPDS card No-42-1467). These peak positions assigned to Co_3O_4 are also in agreement with those reported by Zhang *et al.* on their 3d nanosheet arrays of Co-Co_3O_4 prepared by a potentiostatic deposition process [23] as well as those reported by Duraisamy *et al.* on their Co_3O_4

nanoparticles synthesized by a pyrolysis technique [24]. Similar peak positions have also been reported by Bin Qui *et al.* for Co_3O_4 and Co-CoO-C materials prepared by a potentiodynamic mode of electrodeposition [25]. The peaks marked with asterisks '*' originate from the Ti-substrate and are attributable to Ti (100), Ti (002) and Ti (101) planes (JCPDS card No-00-005-0682).

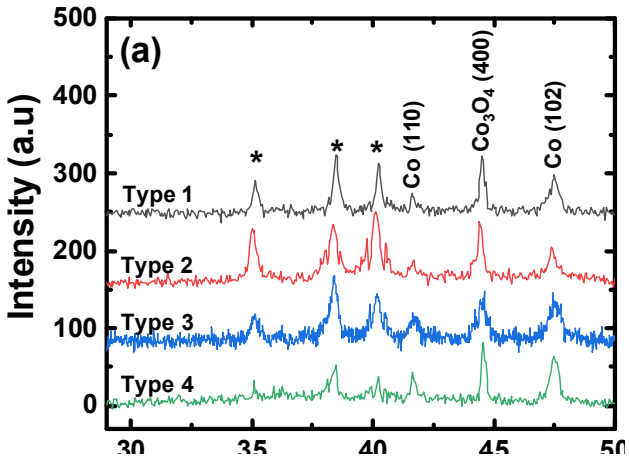

Figure 2. XRD patterns of Type 1, 2, 3, and 4 Co-Co_3O_4 nanocomposite thin films synthesized by CV, CVPS +1.0V, CVPS –1.4V and CVPRP electrodeposition modes on Ti-substrate

All the four types of thin films electrodeposited on NF substrates were analyzed by FTIR spectrometry for confirming the formation of Co_3O_4 following the deposition processes employed. The FTIR spectra obtained from these thin films within the range of interest between 500 and 1000 cm^{-1} are presented in Figure 3(a). Two absorption bands observed in the wavenumber range of 646-658 cm^{-1} and 530-554 cm^{-1} are attributed to the stretching vibrations of Co-O bond in the tetrahedrally and octahedrally coordinated cobalt, respectively. The presence of these fingerprint absorption bands confirms the formation of Co_3O_4 for all the four types of thin films electrodeposited under the four different modes

briefed in Table 1. The wavenumber ranges within which these absorption bands appear are also in good agreement with reports in the literature [15, 18, 26-28]. While the formation of Co_3O_4 is evident from the IR absorption bands in Figure 3(a), the intensities of these bands are obviously varying. Therefore, in order to understand the oxide peak intensities and their possible effect on the supercapacitive behavior of these thin films, we further investigated the area under these two representative peaks and are presented in Figure 3(b). The area under the peaks clearly vary for different electrodeposition modes used and least area under the peak is observed in particular on the Type 3 thin film (CV PS -1.4V). It is possible that in the Type 3 thin film, due to the negative potential used in the deposition process, metal layers are deposited resulting in lower intensity of the oxide. Therefore, it can be expected that the specific capacitance can vary depending on the oxide intensities revealed by the FTIR peak area analysis.

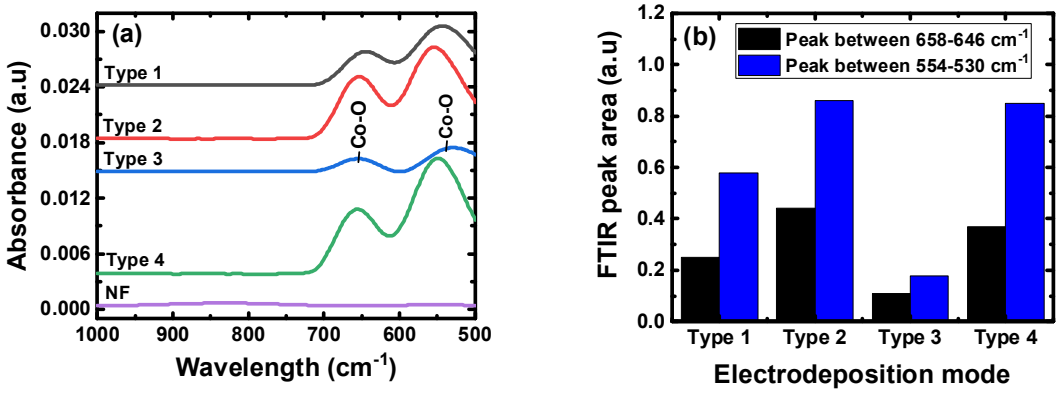

Figure 3. (a) FTIR spectra and (b) area under the two IR absorption bands of Type 1, 2, 3 and 4 Co-Co_3O_4 nanocomposite thin films synthesized by Type 1 (CV), Type 2 (CV PS +1.0V), Type 3 (CV PS – 1.4V) and Type 4 (CVPRP) electrodeposition modes on NF substrate

In addition to the type of oxides and their quantities, it has been reported that the specific surface area resulting from the final morphology and structure of the obtained thin films can have a significant impact on the supercapacitive behavior of Co_3O_4 based electrodes [15, 22]. Therefore, morphological investigations on the four types of thin films

deposited under different modes on NF were further carried out using SEM imaging and are depicted in Figure 4 (a-d). The apparent morphology of all types looks similar; however, a slight variation is certainly visible. In case of Type 1 (CV, Figure 4(a)) and Type 2 (CVPS +1.0V, Figure 4(d)) thin films, for example, CV process (Type 1) presumably results in the formation of a baseline morphology resembling a network of interconnected nanoflakes while the CVPS +1.0V process (Type 2) maintains the initial baseline produced by the CV process, but with an additional cloudy cluster-like morphology formed over the CV's baseline morphology.

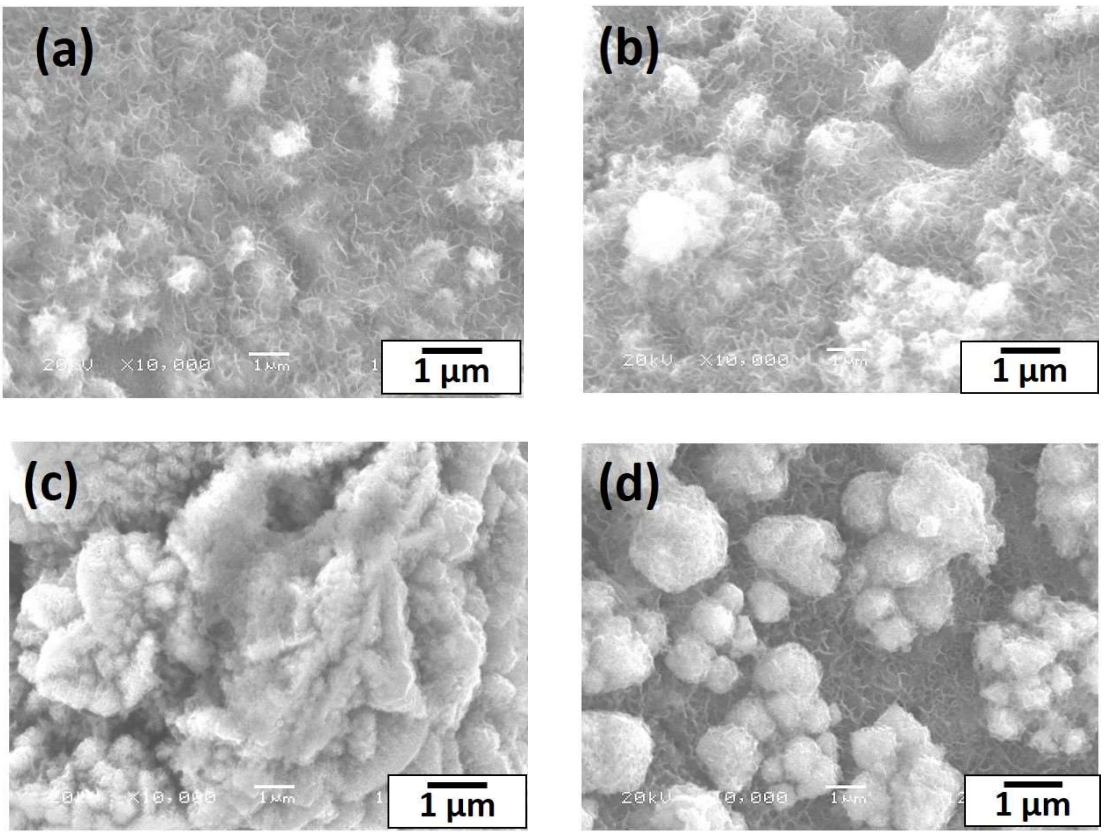

Figure 4. SEM micrographs of the as- synthesized Co-Co_3O_4 nanocomposite thin films on NF substrate prepared by the four different electrodeposition modes: (a) Type 1 (CV), (b) Type 2 (CVPS +1.0V), (c) Type 3 (CVPS –1.4V) and (d) Type 4 (CV PRP)

The surface morphology of the Type 3 thin film deposited by CVPS –1.4V process (Figure 4(c)), however, shows large agglomeration of spongy cloud-like features which may be attributable to overgrowth of the material. This agglomeration may be expected to limit the electrolyte access to the electroactive sites which in turn may affect the capacitive performance. The Type 4 thin film deposited by CV PRP process presented in Figure 4(d), on the other hand, shows well adherent porous interconnected nanoflake morphology decorated with spongy cloud-like features homogenously dispersed over the porous interconnected nanoflakes formed on the substrate. The Type 4 thin film's morphological features may contribute to enhanced surface area favorable for improved access of electrolyte to the electroactive sites and hence increase the capacitive ability [11, 29]. Morphological features resembling that of our thin films obtained via the four modes of electrodeposition process has been previously reported by Jagadale *et al.* presenting nanoflake-like mesoporous cobalt oxide film prepared by potentiodynamic, galvanostatic and potentiostatic modes of electrodeposition [15].

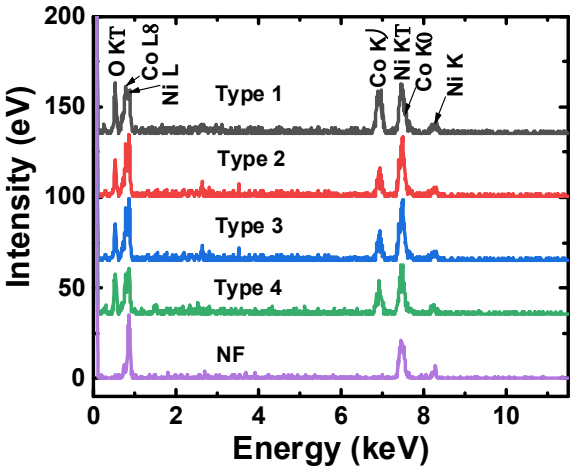

Figure 5. EDX spectra of NF substrate and Type 1 (CV), Type 2 (CV PS +1.0V), Type 3 (CV PS –1.4V) and Type 4 (CV PRP) Co-Co_3O_4 nanocomposite thin films on NF substrate

During the SEM image analysis, EDX spectra (Figure 5) were also collected on all the four types of thin films as well as on the NF substrate in complementing the FTIR spectral analysis for the confirmation of the presence of oxide on these films. All the elements of interest were traced on the EDX spectra, including O, Co and Ni, where Ni arises from the NF substrate. The presence of O in all the four thin film types and absence of O on NF substrate confirms the oxide formation on the electrodeposited thin films surfaces. The atomic ratio of O to Co (O/Co) for Type 1, Type 2, Type 3 and Type 4 thin films are found to be 1.9, 2.1, 1.7 and 3.0 respectively, with a close match with the Co_3O_4 stoichiometric as supported by the study of Faisal Ali *et al.*. [16]. The Type 4 thin film deposited by CVPRP process, however, shows reasonably higher O/Co ratio indicating that this thin film may result in a higher specific capacitance value. Additionally, a comparison of the EDX point scans of the film (beneath the sponge-like features) and sponge like material presented in the Figure S1 of the supplementary shows that, the O/Co ratio of 2.4 in the film beneath the sponge-like features is higher compared to O/C ratio of 1.4 on the sponge-like material. The O/Co ratio of Co_3O_4 theoretically is 1.33 (4/3), which is very close to the value obtained on the EDX point scan of the sponge-like features. Therefore, it may be assumed that these sponge-like features are mostly Co_3O_4 and therefore may contribute to high specific capacitance.

Figure 6(a) shows the CV curves of the four types of Co-Co_3O_4 nanocomposite thin films deposited by Type 1 (CV), Type 2 (CV PS +1V), Type 3 (CV PS -1.4V) and Type 4 (CV PRP) modes of electrodeposition on NF substrates at a scan rate of 5 mV/s. Also, the CV curves of the various types of Co-Co_3O_4 nanocomposite thin films at different scan rates (100, 50, 20, 10 and 5 mV/s) have been presented in Figure S2 of the supplementary data. The shapes of the CV curves show that the as-synthesized Co-Co_3O_4 nanocomposite thin films deposited by the Type 1, Type 2, Type 3 and Type 4 modes of electrodeposition are strongly governed by faradaic processes and presents both anodic (oxidation) and cathodic (reduction) peaks from the Co-Co_3O_4 thin film electrodes [4].

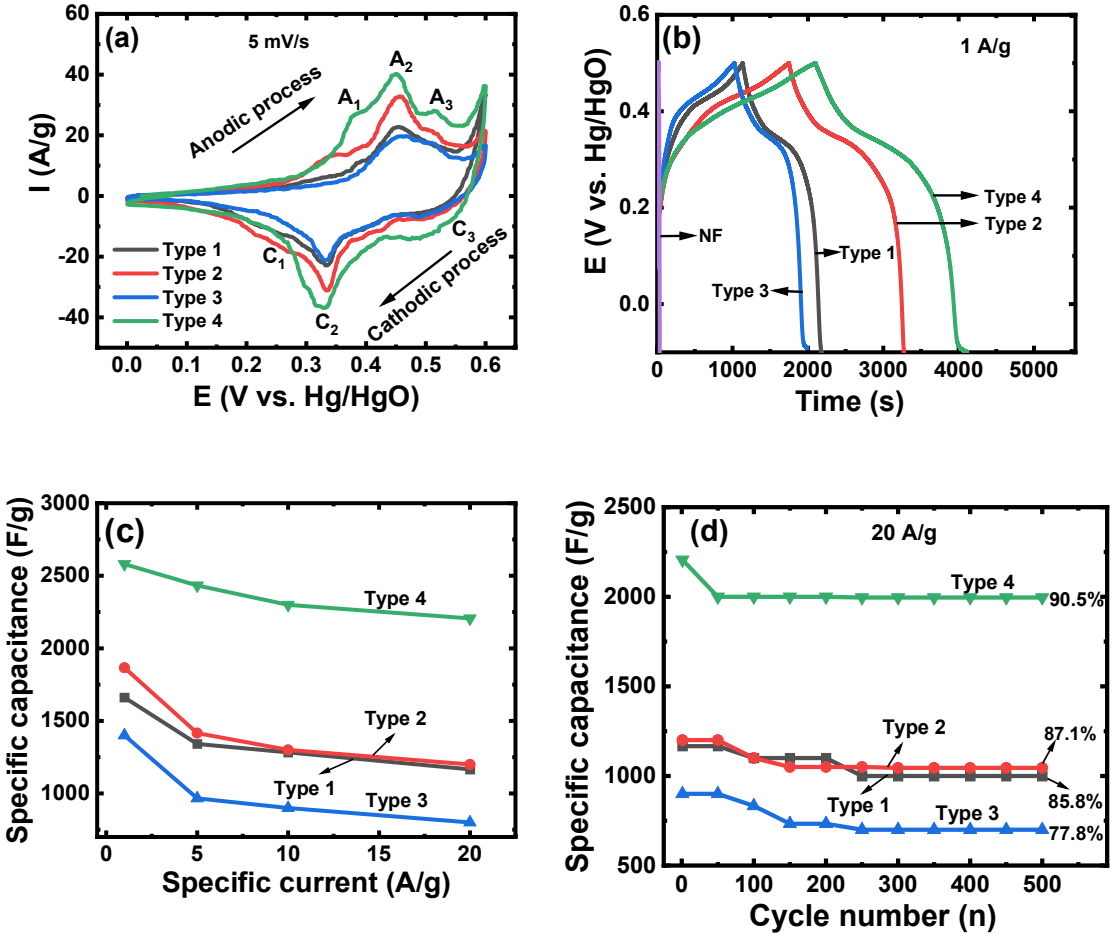

Figure 6. (a) Cyclic voltammetry curves at 5mV/s, (b) Charge-discharge curves at 1 A/g, (c) Variation of specific capacitance at different specific current graph (d) Cycling performance for 500 cycles at a specific current of 20 A/g of the Type 1 (CV), Type 2 (CV PS +1V), Type 3 (CV PS -1.4V) and Type 4 (CV PRP) Co-Co_3O_4 nanocomposite thin films on NF substrate.

The first redox peak (A1 (0.38V), C1 (0.24V)) and the third redox peaks (A3 (0.52V), C3 (0.51V)) can be correlated to the redox reaction of Co^{2+}/Co^{3+} as depicted in Equation (1) [30]. The second pair of redox peaks (A2 (0.45V), C2 (0.33V) is correlated to the redox reaction of Co^{3+}/Co^{4+} shown in equation 2 [30, 31].

$$Co_3O_4 + H_2O + OH^- \leftrightarrow 3CoOOH + e^- \quad (1)$$

$$CoOOH + OH^- \leftrightarrow CoO_2 + H_2O + e^- \quad (2)$$

It can be noted that the CV curve of the Type 4 film presents higher area under the CV curve as compared to the other modes of electrodeposition. The larger area indicates a higher accumulation of charge at the CVPRP thin film electrode surface during potential cycling process, and therefore expected to show higher specific capacitance.

The GCD curves of the four types of Co-Co_3O_4 nanocomposite thin films as well as the bare NF substrate at a specific current of 1 A/g are presented in Figure 6(b). The nonlinear nature of the GCD curves shows the pseudocapacitive nature of the Co-Co_3O_4 thin film electrodes. Note that all types of Co-Co_3O_4 nanocomposite thin films do not exhibit significant potential drop (V_{IR}) between the charge and discharge curves, implying good conductivity. It is evident that the Type 4 thin film electrode (CV PRP mode) possesses longer discharge curves compared to the other three types of thin film electrodes indicating that the Type 4 electrode may show higher specific capacitance value. The specific capacitance estimated from the GCD curves are 1661, 1866, 1400 and 2580 F/g for the Type 1 (CV), Type 2 (CV PS +1.0V), Type 3 (CV PS –1.4V) and Type 4 (CV PRP), respectively at a current load of 1 A/g using equation 3,

$$C = \frac{I\Delta t}{m\Delta V} \quad (3)$$

where *C* is the specific capacitance, *I* is the specific current, *Δt* is the discharge time, *m* is the electrode mass, and ΔV is the potential change during discharge. These specific capacitance values for Types 1 to 4 are much higher than previously reported values. Aboelazm *et al.* reported a specific capacitance value of 1273 F/g at 1 A/g for their hierarchical Co_3O_4 nanostructures prepared by magnetic electrodeposition at a constant voltage of -1.0 V for 20 s on nickel foam [32]. Zhang *et al.* reported a specific capacitance value of 1520 F/g at 1 A/g on their Co-Co_3O_4 nanosheet arrays deposited on activated carbon cloth by electrodeposition and a post annealing at 400 ºC [23]. Specific capacitance values much lower than these authors have been reported on Co_3O_4 electrodes on different substrate materials prepared by various other fabrication techniques as reported in a review by Uke *et al.* [2]. The GCD curves were used for the quantitative analysis while the CV

curves were used (Figure 6(a)) for qualitative understanding of the expected specific capacitance behavior.

Figure 6(c) shows the capacitance variation of the four types of thin film electrodes at the specific currents of 1, 5, 10 and 20 A/g. The specific capacitance is found to decrease with the increasing current density possibly due the minimum electrolytic contact with the electrode material at higher current densities. At higher constant discharge currents, the OH^- ions from the electrolyte reach only the outer surface of the electrode; thus, the electrode material at the inner surface does not get fully involved in the electrochemical reactions resulting in lower specific capacitance. This phenomenon where low specific capacitance values are attributed to the poor electrochemical reactivity between the electrolytes and the electrode materials has been commonly observed by other authors [2, 15, 29, 30].

The high capacitance of the Type 4 (CV PRP) thin film electrode could be attributed to the interconnected nanoflake-like morphology decorated with cloudy structures providing maximum surface area at electrode/electrolyte interface. Additionally, the higher O/Co atomic ratio obtained from the EDX compositional analysis may also contribute to the high charge storage capacity. The dependence of the specific capacitance on the oxide content in the electrode material was confirmed by the EDX compositional analysis as shown in Figure 7. It is clear from the graph that higher O/Co atomic ratio indicating higher oxide content in the electrode thin films show higher specific capacitance.

While electrode materials with high specific capacitance is important, the long-term cycling stability is another important aspect in practical applications of supercapacitors. The cycling performance of the four types of thin film electrodes deposited on NF substrate under four different electrodeposition modes was, therefore, evaluated and is presented in Figure 6(d). The cyclic performance was evaluated by conducting charge-discharge measurements at a current load of 20 A/g for 500 cycles. The specific capacitance retention was found to be 77.8% for Type 1 (CV only), 87.1% for Type 2 (CV +1.0V), and 85.8% for Type 3 (CV -1.4V) thin films while the Type 4 (CV PRP) shows maximum retention of 90.5% after 500 cycles.

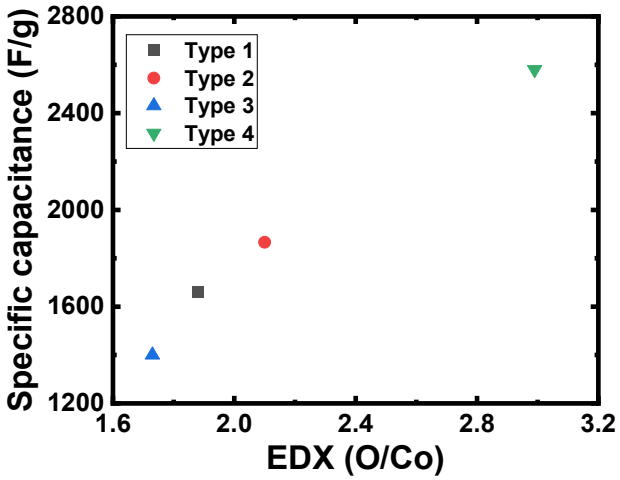

Figure 7. Variation of specific capacitance as a function of O/Co atomic ratio obtained from EDX analysis for Type 1 (CV), Type 2 (CV PS +1V), Type 3 (CV PS -1.4V) and Type 4 (CV PRP) Co- Co_3O_4 nanocomposite thin films on NF substrate.

The high specific capacitance as well as its maximum retention of Type 4 thin films as compared to the other types which show relatively lower specific capacitance and retention demonstrates as ideal combination for practical applications while the ease of developing these thin film electrodes shows promises to future large-scale manufacturing. The SEM image and the CV curve at 5 mV/s for the Type 4 thin film after 500 GCD cycles have been presented in Figure S3 of the supplementary data.

In addition to the specific capacitance investigations, electrochemical impedance spectroscopy (EIS) was also carried out to investigate the charge kinetic properties of the electrode in a frequency range from 10 mHz to 100 kHz.. Figure 8(a) shows Nyquist plots of the Co-Co_3O_4 nanocomposite thin films electrodes deposited by the four different electrodeposition modes. All four types apparently present almost straight lines with maximum slope for type 4 (CV PRP) with nearly vertical line. The slopes 1.7, 3.3, 1.9 and 5.4 for Type 1, Type 2, Type 3 and Type 4 respectively change systematically and is found

complementary with the obtained specific capacitance of the electrodes. The electrode with capacitive characteristic shows higher slope, for example in case of Type 4 [14]. Type 4 shows a nearly vertical straight line compared to the others indicating better capacitor behaviour. Figure 8(b) and (c) shows the Bode plots of the four types of the thin film electrodes. At very high frequencies, the intercept of the plot with the X-axis represents the equivalent series resistance (ESR) as shown in Figure 8(b), which is a combination of the electrolyte resistance, the intrinsic resistance of the active material, and the contact resistance at the electrode-electrolyte interface [9]. The ESR values of all four types of thin films are found to be very low. This lower ESR value could be the result of the increased surface area of the deposited composite electrode thin film structure with good electrical conducting properties [33]. Figure 8(b) shows the impedance of the four electrode types. The Type 4 (CV PRP) electrode shows a lower impedance compared to the other three electrode types. The Bode plot in Figure 8(c) describes the relationship between phase angle and frequency which shows that the four electrodes electrodeposited by Type 1, Type 2, Type 3 and Type 4 respectively processes exhibit a good capacitive performance at phase angles 55.9 °, 64.9 ° 54.6 ° and 71.7 °, respectively [14]. A phase angle of 90° is typically observed only in EDLCs using carbon materials whereas deviations from 90° are commonly observed in pseudocapacitors. The relaxation time (τ) in seconds (s) was calculated using the following equation (4):

$$\tau = \frac{1}{f_o} \tag{4}$$

where (f_o) is frequency at the phase angle of 45 ° and they were computed to be 0.10, 0.62, 1.10 and 0.60 s for Type 1, Type 2, Type 3 and Type 4, respectively (Figure 8(c)). Shorter relaxation time indicates that electrode could switch more rapidly from resistive behavior to capacitive behavior [32].

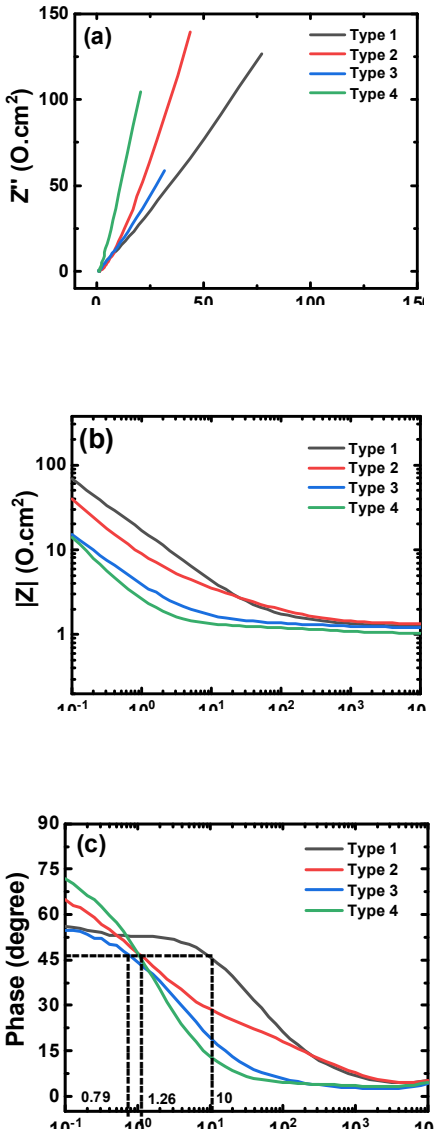

Figure. 8. (a) Nyquist plots, (b) Bode plot of the frequency's dependence on the impedance magnitude (|Z|), (c) Bode plots of the frequency's dependence on the phase angle of the Type 1 (CV), Type 2 (CV PS +1V), Type 3 (CV PS -1.4V) and Type 4 (CV PRP) Co-Co_3O_4 nanocomposite thin films synthesized on NF substrate.

4 | Conclusion

Co-Co_3O_4 nanocomposite thin films electrode materials have been synthesized on nickel foam (NF) substrates using four different electrodeposition modes, namely, cyclic voltammetry (CV), combination of cyclic voltammetry and potentiostatic at –1.4 V (CV PS –1.4V), combination of cyclic voltammetry and potentiostatic at 1.0 V (CV PS +1.0V) and combination of cyclic voltammetry and pulse reverse potential (CV PRP). The XRD patterns have confirmed the presence of Co and Co_3O_4 on all the electrodes. The chemical nature of the electrode thin films has been complemented by the presence of Co_3O_4 absorption bands and strong oxygen peak intensities on the FTIR and EDX spectra respectively. The SEM images have revealed porous microfeatures which changes slightly for different electrodeposition modes, fulfilling the important criterion of its contributing to large specific surface area of the electrode surfaces. The Type 4 film synthesized by combining cyclic voltammetry and pulse reverse potential processes (CV PRP) is found to have resulted in a maximum specific capacitance of 2580 F/g while the Types 1, 2 and 3 thin films deposited by cyclic voltammetry (CV), combination of cyclic voltammetry and potentiostatic at –1.4 V (CVPS –1.4V), combination of cyclic voltammetry and potentiostatic at 1.0 V (CVPS +1.0V) have resulted in specific capacitance values of 1661, 1400, 1866 F/g respectively. Their respective capacitance retention for Type 1, 2, 3 and 4 thin film electrodes have been found to be 85.8, 77.8, 87.1, and 90.5 %, after 500 cycles of charging/discharging under a high current load of 20 A/g. Comparative analysis shows that the Type 4 thin film electrode material electrodeposited by CV PRP process has a greater potential as high-performance supercapacitor material in terms of high specific capacitance and charging/discharging cycle stability. These results and observations place the Type 4 (CV PRP) electrode as ideal material for practical applications and shows promises to future large-scale manufacturing due to the ease of fabrication of these thin films.

ACKNOWLEDGEMENT

We acknowledge the financial support provided by the Natural Sciences and Engineering Research Council of Canada (NSERC). We thank Dr. Stephan Simard for donating us the electrochemical measurement equipment.

REFERENCES

1. Mohd Abdah MAA, Azman NHN, Kulandaivalu S, Sulaiman Y. Review of the use of transition-metal-oxide and conducting polymer-based fibres for high-performance supercapacitors. ***Mater Des***. 2020;186:108199.
2. Uke SJ, Akhare VP, Bambole DR, Bodade AB, Chaudhari GN. Recent Advancements in the Cobalt Oxides, Manganese Oxides, and Their Composite As an Electrode Material for Supercapacitor: A Review. ***Front Mater***. 2017;4:21.
3. Sivakumar P, Raj CJ, Opar DO, Park J, Jung H. Two dimensional layered nickel cobaltite nanosheets as an efficient electrode material for high-performance hybrid supercapacitor. ***Int J Energy Res***. 2021:1–11.
4. Zhu H, Liu J, Zhang Q, Wei J. High electrochemical performance of metal azolate framework-derived ZnO/Co3O4 for supercapacitors. ***Int J Energy Res***. 2020;44:8654-8665.
5. Jagadale AD, Kumbhar VS, Lokhande CD. Supercapacitive activities of potentiodynamically deposited nanoflakes of cobalt oxide (Co3O4) thin film electrode. ***J Colloid Interface Sci***. 2013;406:225-230.
6. Meher SK, Rao GR. Ultralayered Co3O4 for High-Performance Supercapacitor Applications. ***J Phys Chem C***. 2011;115:15646-15654.
7. Liang R, Du Y, Xiao P, Cheng J, Yuan S, Chen Y, Yuan J, Chen J. Transition Metal Oxide Electrode Materials for Supercapacitors: A Review of Recent Developments. ***Nanomaterials*** 2021;11:1248.
8. Ali F, Khalid NR, Nabi G, Ul-Hamid A, Ikram M. Hydrothermal synthesis of cerium-doped Co3O4 nanoflakes as electrode for supercapacitor application. ***Int J Energy Res***. 2020;45:1999-2010.
9. Mohamed SG, Attia SY, Hassan HH. Spinel-structured FeCo2O4 mesoporous nanosheets as efficient electrode for supercapacitor applications. ***Microporous Mesoporous Mater***. 2017;251:26-33.
10. Gao M, Wang WK, Rong Q, Jiang J, Zhang YJ, Yu HQ. Porous ZnO-Coated Co3O4 Nanorod as a High-Energy-Density Supercapacitor Material. ***ACS Appl Mater Interfaces***. 2018;10:23163-23173.
11. Mei J, Fu W, Zhang Z, Jiang X, Bu H, Jiang C, Xie E, Han W. Vertically-aligned Co3O4 nanowires interconnected with Co(OH)2 nanosheets as supercapacitor electrode. ***Energy***. 2017;139:1153-1158.
12. Yan X, Tian L, He M, Chen X. Three-Dimensional Crystalline/Amorphous Co/Co3O4 Core/Shell Nanosheets as Efficient Electrocatalysts for the Hydrogen Evolution Reaction. ***Nano Lett***. 2015;15:6015-6021.
13. Yousefi SR, Alshamsi HA, Amiri O, Salavati-Niasari M. Synthesis, characterization and application of Co/Co3O4 nanocomposites as an effective photocatalyst for discoloration of organic dye contaminants in wastewater and antibacterial properties. ***J Mol Liq***. 2021;337:116405.
14. Harilal M, Krishnan SG, Vijayan BL, Venkatashamy Reddy M, Adams S, Barron AR, Yusoff MM, Jose R. Continuous nanobelts of nickel oxide–cobalt oxide hybrid with improved capacitive charge storage properties. ***Mater Des***. 2017;122:376-384.

15. Jagadale AD, Kumbhar VS, Bulakhe RN, Lokhande CD. Influence of electrodeposition modes on the supercapacitive performance of Co3O4 electrodes. ***Energy***. 2014;64:234-241.
16. Ali F, Khalid NR. Facile synthesis and properties of chromium-doped cobalt oxide (Cr-doped Co3O4) nanostructures for supercapacitor applications. ***Appl Nanosci***. 2020;10:1481-1488.
17. García-Gómez A, Eugénio S, Duarte RG, Silva TM, Carmezim MJ, Montemor MF. Electrodeposited reduced-graphene oxide/cobalt oxide electrodes for charge storage applications. ***Appl Surf Sci***. 2016;382:34-40.
18. Lima-Tenório MK, Ferreira CS, Rebelo QHF, Souza RFBd, Passos RR, Pineda EAG, Pocrifka LA. Pseudocapacitance Properties of Co3O4 Nanoparticles Synthesized Using a Modified Sol-Gel Method. ***Mater Res***. 2018;21:e20170521.
19. Cheng JP, Chen X, Wu J-S, Liu F, Zhang XB, Dravid VP. Porous cobalt oxides with tunable hierarchical morphologies for supercapacitor electrodes. ***CrystEngComm***. 2012;14:6702–6709.
20. Li Y, Li X, Wang Z, Guo H, Li T. Distinct impact of cobalt salt type on the morphology, microstructure, and electrochemical properties of Co3O4 synthesized by ultrasonic spray pyrolysis. ***J Alloys Compd***. 2017;696:836-843.
21. Valatka E, KelpŠAitĖ I, BaltruŠAitis J. Electrochemical Deposition of Porous Cobalt Oxide Films on AISI 304 Type Steel. ***Mater Sci***. 2011;17:236-243.
22. Aghazadeh M, Hosseinifard M, Sabour B, Dalvand S. Pulse electrochemical synthesis of capsule-like nanostructures of Co3O4 and investigation of their capacitive performance. ***Appl Surf Sci***. 2013;287:187-194.
23. Zhang M, Xu Y, Fan H, Zhao N, Yan B, Wang C, Ma J, Yadav AK, Zhang W, Du Z, Zheng X, Li M, Dong G, Wang W. In situ synthesis of 3D Co@Co3O4 nanosheet arrays for hybrid supercapacitors with ultra-high rate performance. ***J Alloys Compd***. 2020;826:154115.
24. Duraisamy E, Gurunathan P, Das HT, Ramesha K, Elumalai P. [Co(salen)] derived Co/Co3O4 nanoparticle@carbon matrix as high-performance electrode for energy storage applications. ***J Power Sources***. 2017;344:103-110.
25. Qiu B, Guo W, Liang Z, Xia W, Gao S, Wang Q, Yu X, Zhao R, Zou R. Fabrication of Co3O4 nanoparticles in thin porous carbon shells from metal–organic frameworks for enhanced electrochemical performance. ***RSC Adv***. 2017;7:13340-13346.
26. Cai H, Wei Q, Xiao H, Liu H, Wang J. Preparation and microwave absorption properties of petal CoO/CNFs composites. ***J Mater Sci: Mater Electron***. 2020;31:7606-7615.
27. Liu F, Su H, Jin L, Zhang H, Chu X, Yang W. Facile synthesis of ultrafine cobalt oxide nanoparticles for high-performance supercapacitors. ***J Colloid Interface Sci***. 2017;505:796-804.
28. Aadil M, Zulfiqar S, Shahid M, Haider S, Shakir I, Warsi MF. Binder free mesoporous Ag-doped Co3O4 nanosheets with outstanding cyclic stability and rate capability for advanced supercapacitor applications. ***J Alloys Compd***. 2020;844:156062.
29. Rusi, Chan PY, Majid SR. Layer by Layer Ex-Situ Deposited Cobalt-Manganese Oxide as Composite Electrode Material for Electrochemical Capacitor. ***PloS one***. 2015;10:e0129780.

30. Mirzaeian M, Akhanova N, Gabdullin M, Kalkozova Z, Tulegenova A, Nurbolat S, Abdullin K. Improvement of the Pseudocapacitive Performance of Cobalt Oxide-Based Electrodes for Electrochemical Capacitors. ***Energies***. 2020;13:5228.
31. Zhang F, Yuan C, Lu X, Zhang L, Che Q, Zhang X. Facile growth of mesoporous Co3O4 nanowire arrays on Ni foam for high performance electrochemical capacitors. ***J Power Sources***. 2012;203:250-256.
32. Aboelazm EAA, Ali GAM, Algarni H, Yin H, Zhong YL, Chong KF. Magnetic Electrodeposition of the Hierarchical Cobalt Oxide Nanostructure from Spent Lithium-Ion Batteries: Its Application as a Supercapacitor Electrode. ***J Phys Chem C***. 2018;122:12200-12206.
33. Rusi, Majid SR. Effects of Electrodeposition Mode and Deposition Cycle on the Electrochemical Performance of MnO2-NiO Composite Electrodes for High-Energy-Density Supercapacitors. ***PloS one***. 2016;11:e0154566.